On the use of shape memory alloys for deployable passive heat radiators in space satellites

A Bacciotti[1], F Bucchi[*,1], F Frendo[1], M Mameli[2], R Perna[2], S Filippeschi[2]

[1] Department of Civil and Industrial Engineering, University of Pisa, Largo Lucio Lazzarino, 56122, Pisa

[2] Department of Energy, System, Territory and Construction, University of Pisa, Largo Lucio Lazzarino, 56122, Pisa

E-mail: [*]francesco.bucchi@unipi.it

Abstract. The present work presents a multifunctional structure for space engineering application part of the TOPDESS project, funded by ESA.
The main aim of the project is the design of a thermal control device able to deploy through passive actuation. A combined device has been designed, made up of a Pulsating Heat Pipe (PHP) foldable heat exchanger and Shape Memory Alloy (SMA) wire. The deployment of the SMA wire is conceived to be controlled by thermal contact with the heat source and by conduction along the wire. Since the heat sources are lumped and the wire is subject to convection, a temperature gradient develops along the wire.
A monodimensional mode able to predict the behavior of an SMA wire subjected to a spatial temperature gradient, is presented in this paper.
The results show that the system can carry out folding and unfolding cycles with rotation angles greater than 80° only if the wire is subjected to uniform temperature distribution; in the case of temperature gradient, the achievable rotation angle is about 20°.
The analysis states the feasibility of the actuation system, highlighting the critical technological aspects, to lay the groundwork for the future development of the whole system.

1. Introduction

The device presented in this paper is part of the TOPDESS project, funded by ESA. The main aim of the project is the design of a thermal control device for space application able to deploy through passive actuation. The present application proposes a combined passive device, made up of a metal Pulsating Heat Pipe (PHP) foldable heat exchanger and a Shape Memory Alloy (SMA) wire aimed at deploying the structure. The activation of the SMA wire is conceived to be controlled by the thermal contact with the heat source of the heat transfer device and by pure conduction along the SMA wire.
Recent research work has shown that SMA actuators provide an excellent technological opportunity to replace conventional actuators, such as electric motors, pneumatics and hydraulics, due to their characteristics and capability to react directly to external environmental stimuli. Smart systems and, therefore, SMA actuators, promote the development of more advanced and cheaper actuators with a significant reduction in mechanical complexity, size, mass, cost and power consumption, while improving efficiency, and versatility [1]. The Shape Memory Effect (SME) is a peculiar property of SMA, based on martensite transformation, which

allow to recover a preset, memorized, macroscopic shape, with up to 8% of recoverable strain [1], as a result of a mechanical loading followed by a temperature change.
From the standpoint of thermal control equipment, Pulsating Heat Pipes (PHP) are selected as heat exchanger. The PHP is a two-phase passive heat transfer device suitable for high heat flux applications, able to operate in microgravity or against gravity conditions. The basic structure consists of a capillary tube bent turn by turn, which is firstly evacuated, then partially filled with a working fluid and finally sealed. Under operating condition, the tube-bundle of a PHP receives heat at one end, named evaporator section, and it is cooled at the other, named condenser section. The working fluid evaporates near the hot section, with vapor bubbles generation and growth, and, simultaneously, bubbles collapse and shrink, due to condensation, in the condenser. The resulting effect of the action of bubbles represents the pumping force needed to move slugs or bubbles to locations where evaporation and condensation can occur, and the device is able to passively transfer latent and sensible heat. The main physical phenomena characterizing the working principle of a generic PHP are the phase change and the capillarity. In particular, the evaporation of the liquid causes the vapor plug expansion in the channel, which is the triggering phenomenon for the fluid circulation. On the other hand, the capillarity gives an essential contribution not so much for driving the fluid in the tubes, but rather to the imposition of a slug flow pattern. Smart actuation systems based on SME are employed in industrial and commercial applications in the field of biomedical, robotic, mechanical and aerospace. To the best of the authors knowledge, the following papers consider SME applications to foldable structure or aerospace environment. Katayama et al. [2] describe a hinge mechanism actuated by SMA wires for deploying segmented plates. NiTi based alloy is employed and the wires are elongated and uniformly heated by means of an infrared quartz lamp to simulate solar radiations. Tension develops in the wire during the recovery, yielding a moment about the hinge that causes the angular displacement of the moving plate. Carpenter et al. [3] consider the Lightweight Flexible Solar Arrays (LFSA) technology for space applications, that has innovative features about exploited solar cells and about the use of SMAs as actuators for a shockless deployment of the solar panels. The NiTi alloy strips, uniformly heated by means of external heaters, are forced to bend allowing the angular displacement of the panels. The Folded Lightweight Actuated Positioning System (FLAPS), by Vale Pereira et al. [4], demonstrates the use of a rotary shape memory alloy actuator for CubeSats. The mechanism consists of a pair of NiTi SMA strip actuators activated by Joule effect and mounted to a hinge assembly. The actuators allow repeatable movement of the deployable element in two directions: one strip actuates to deploy the mechanism, and the other strip brings it back to the stowed position. SMA can also be implemented to deploy telecommunication antenna installed on spacecrafts. This is the case for the antenna designed by Lan et al. [5]. This paper is concerned about the design of an antenna that consists of six deployable ribs connected to a central hub. The hinges are based on NiTi SMA wires, activated by electric current, that act as actuators to deploy the ribs. For what concern robotic applications, the work by Maffiodo et al. [6] presents a flexible robotic finger, composed by a variable number of modules to obtain complex deformation of the finger. The motion of a module is performed by NiTi SMA wires, heated by Joule effect to cause shortening, and cooled to cause stretching. Bertagne et al. [7] present in their work a novel radiator concept that employs SMAs to geometrically reconfigure a radiative panel, enabling the control of both radiator view of space and emissive power. The radiator switches between two shapes thanks to SMA wires that are uniformly heated and cooled to unroll and roll the panel. The Advanced eLectrical Bus (ALBus) project is a technology demonstration mission of a 3U CubeSat that employs SMA technology for reliable solar array deployable mechanisms. The project is presented by Guzik et al. [8]. ALBus CubeSat is designed to deploy four solar arrays by means of a hinge mechanism that exploits NiTi sheet shaped SMAs activated by Joule effect. The work by Akizuki et al. [9] reports the design, fabrication, and testing of a deployable

thermal panel for space applications. The actuation motion is allowed by a SMA-based system. In order to deploy and stow the fin, the CuAlNi SMA wire, uniformly heated by external heaters, pushes out the drive crank and torsion bar to convert the horizontal force into a rotational force. The literature review allows considerations about the trend that engineering is following about the use of SMAs in actuation systems. Strips and sheets replace in some cases the use of wires as actuation means, even if the wire is the most employed configuration due to its simplicity in the modelling and the design. Nickel Titanium based alloys are clearly the most common and the most commercially available choice for what concerns the material involved in smart actuation systems. Today, more than 90% of all the commercial shape memory applications are based on binary NiTi or ternary NiTiCu and NiTiNb alloys [10]. Furthermore, active mechanisms for uniformly heating and activating SMAs, such as electrical current or heaters, are preferred with respect to passive ones. The statement of the present application concerns the implementation of a completely passive system based on SMA wire, that exploits both conductive and radiative heat transfer without any kind of external source implemented on purpose to provide thermal power to the system and activate it. Since the heat sources are lumped and the wire is subject to convection, a temperature gradient is supposed to develop along the wire. For this reason, a monodimensional thermodynamic model, able to predict the temperature distribution of the SMA under the described thermal boundary conditions, is needed and developed. To the best of the authors knowledge, the models that are available in the technical literature present a uniform temperature distribution on the SMA. In the present work a smart monodimensional model, based on an extension of the well-known Brinson model, able to predict the behavior of an SMA wire subjected to a spatial temperature gradient, is presented.

2. Design of the SME actuated foldable heat radiator

The concept of the PHP heat radiator actuated by SMA wire is shown in figures 1–3.

Figure 1 shows the PHP, shaped as torsional spring, in unloaded configuration. Two supports are fixed at the ends of the PHP: one of them is fixed while the other one is mobile, and it is free to rotate.

Once the device is assembled at environmental temperature $T < M_f$ (martensite finish temperature) in closed configuration (figure 2, a preload is imposed to the torsional spring and the SMA wire, initially made up of twinned martensite, is clamped at its ends to the fixed support and to the SMA wire clamp. The SMA wire bends twice near the torsional spring (PHP) by means of two pulleys and is elongated due to the torsional spring preload in order produce the complete detwinning of the martensite. Subsequently, the supports are heated by the PHP in order to produce the complete phase transformation of the SMA wire (from detwinned martensite to austenite). In this way the SMA wire recovers the accumulated deformation, getting shorter and forcing the mobile part of the system to rotate and the whole structure to deploy (figure 3).

2.1. Mechanical model of the PHP torsional spring

The state-of-the-art review about deployable heat exchangers reveals that no options can be exploited to provide enough flexibility (about 90° of angular ration) to metal PHP starting from the classic straight configuration without causing plastic strain of the tubes. A different and innovative configuration of the PHP has then been developed: the idea is to design the adiabatic section of the PHP shaped as a torsional spring. This particular shape, from the mechanical point of view, gives to the metallic device the elastic deformability needed to carry out cycles of angular rotations avoiding plastic deformations. One of the possible configurations for a foldable PHP is represented in figure 4 with the adiabatic section, in green color, shaped as a torsional spring. The condenser section is highlighted by the blue color, while the evaporator section with the red color.

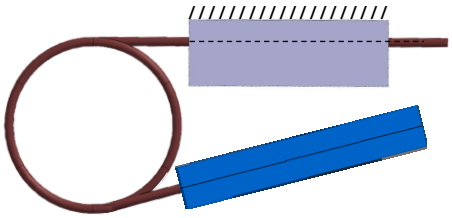

Figure 1. Concept of the PHP heat radiator actuated by SMA wire - Unloaded.

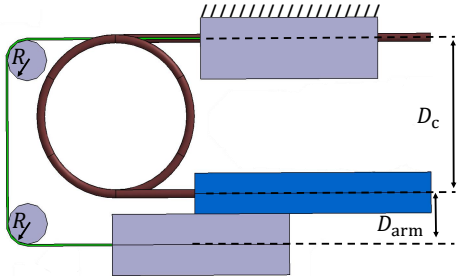

Figure 2. Concept of the PHP heat radiator actuated by SMA wire - Closed.

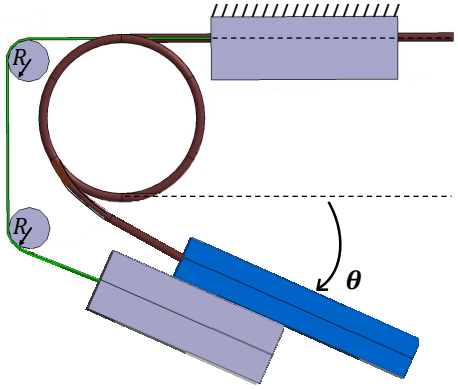

Figure 3. Concept of the PHP heat radiator actuated by SMA wire - Deployed

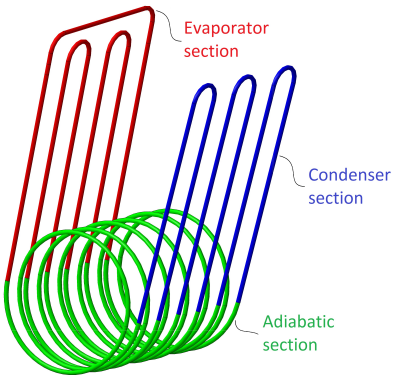

Figure 4. Generic configuration of the coil-shaped PHP.

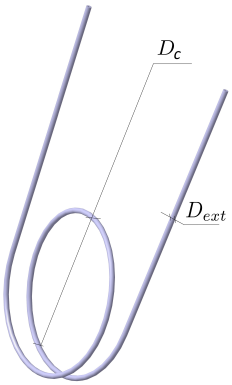

Figure 5. Simplified configuration of the coil-shaped PHP.

In order to compute the stiffness and the allowed rotation of the PHP structure, considering the repetition symmetry of the system, the configuration is simplified, reducing the whole PHP in a single couple of straight arms, spaced by an adiabatic section with a certain number of coils N. The simplified structure is represented in figure 5, where three relevant geometric parameters are shown: the tube external diameter D_{ext}, the tube internal diameter D_{int}, the coil diameter D_c.

The PHP simplified configuration is mechanically studied exploiting the beam theory and

linear elastic material properties; the stiffness k_θ of the torsional spring is

$$k_\theta = \frac{M_{PHP}}{\theta} = \frac{EJ}{N\pi D_c + L_f} \tag{1}$$

where M_{PHP} is the moment applied to the torsional spring, θ is the rotation angle between the two straight parts of the pipe, E is the Young modulus of the pipe material, J is the bending inertia moment of the pipe and L_f is the free length of the straight parts of the pipe subject. In order to guarantee the elastic behavior of the pipe material under the external applied loads, it has to be verified that the maximum stress of the pipe is lower than the admissible stress for the chosen material.
From the mechanical standpoint, the model would suggest the increase of the number of coils to get higher rotation angles, but thermofluidic considerations must suggest to minimize N, since it is directly linked to both local and distributed pressure losses. The helicoidal shape represents an obstacle to the regular circulation of the fluid, since it modifies point by point the momentum path and the fluid velocity direction. The result is an increase of the local pressure losses with respect to the classic straight PHP configuration. On the other hand, the distributed pressure losses are linked to the length of the adiabatic region L_{adiab} of the device. In fact, they are directly proportional to the length of the tube in which the fluid is flowing, since $L_{adiab} = N\pi D_c$. Therefore, the spring model is used in a trade off with thermofluidic considerations about the performance and the working principle of the heat transfer device to fix the relevant geometric parameters and the material properties that must characterized the PHP. Aluminium series 2000 and 7000 are selected to satisfy the imposed requirements and to allow rotations of about 90°.

2.2. Mechanical model of SME

To simulate and predict the shape memory effect and the pseudoelastic behavior of SMAs, numerous studies [1] have been carried out in recent years to develop an efficient mathematical model for SMAs, whose physical behaviour is a function of three variables: stress, strain and temperature. The resulting models can be divided in two categories: micromodels [11, 12, 13] and phenomenological macromodels [14, 15, 16, 17]. In general, micromechanical-based models utilize information about the microstructure of the SMA to predict the macroscopic response. Micromechanical models are useful in understanding the fundamental phenomena of SMA, although they may not be easily implemented for engineering applications. On the other hand, phenomenological models use the principles of continuum thermodynamics to describe the material response. They are calibrated by a limited number of parameters measured at the macroscopic scale through experimental observations, and thus, they are less time consuming from the computational point of view.
To simulate the response of the proposed system actuated by SMAs, the Brinson model [16], subsequently modified by Chung [18], is assumed. This model is a material model capable of representing both the shape memory effect and pseudoelastic behavior by separating the martensite volume fraction ζ into two parts: stress-induced martensite ζ_S and temperature induced martensite ζ_T. This model uses cosine functions for the martensite transformation kinetics, and it needs as inputs four transformation temperatures, martensite start and finish temperatures (M_s and M_f, respectively) and austenite start and finish temperatures (A_s and A_f, respectively), and the critical stresses that define the detwinning process. Exploiting external loads, it is possible to reorient the martensitic variants inducing the transformation from twinned to detwinned martensite. The detwinning process results in a macroscopic shape change, where the deformation is maintained when the load is released. The minimum stress required for detwinning initiation is called detwinning start stress (σ^s_{cr}), while the stress level that corresponds to a complete detwinning of martensite is called detwinning finish stress (σ^f_{cr}). Upon heating

above the characteristic temperature A_f, the phase transformation from detwinned martensite to austenite is completed and the SMA is able to recover the accumulated strain.

With reference to figure6, on the basis of the values of the stress σ and the temperature T, the state of the material can be obtained and, consequently, the martensite fractions ζ_S and ζ_T can be computed. The relationship between each σ-T state and the corresponding martensite

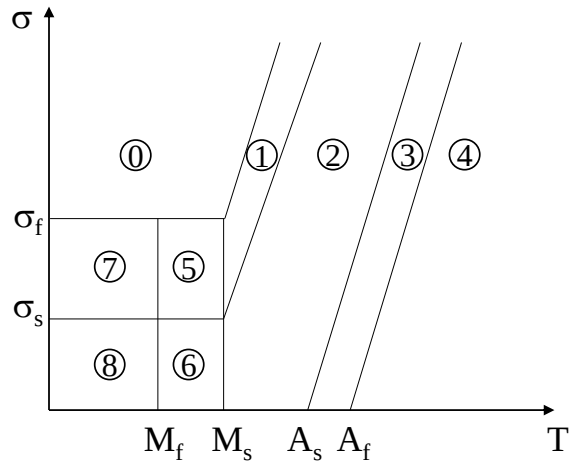

Figure 6. SMA phase diagram.

fractions ζ_S and ζ_T is described in [19].

Once the volume fractions are known, the equivalent deformation ε can be computed, neglecting the thermal deformation, considering the SMA constitutive equation:

$$\varepsilon = \frac{\sigma}{E} + \varepsilon_L \zeta_S \tag{2}$$

where ε_L is the maximum detwinning strain, and E is the Youngs modulus, defined as

$$E = E_A + (E_M - E_A)\zeta \tag{3}$$

4 with E_M and E_A the Young's modulus of the martensite and austenite phase, respectively.

3. Simulation of structure deployment

In order to compute the device deployment under the effect of the SMA wire heating, equilibrium, constitutive and congruence equations have to be considered simultaneously. In fact, the main parameters, the strain of the wire, the stress in the wire and the angle of rotation, are dependent on each other. With reference to figure 7 which represent the , the equilibrium equation is

$$M_{PHP}(\theta) - F_{SMA}(\zeta_S, \zeta_T) d_{arm} = 0 \tag{4}$$

where M_{PHP} is the bending moment of the coil-shaped PHP, F_{SMA} is the force exerted by the SMA wire and d_{arm} is the distance between the wire and the PHP mobile straight arm clamp.

The constitutive equation describing the bending moment as a function of the rotation angle of the mobile arm of the PHP can be obtained from Eq. 4, while the SMA wire force is obtained once the SMA wire stress is known, as expressed in Eq. 2.

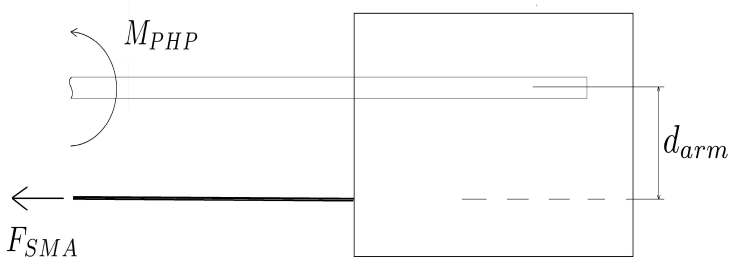

Figure 7. Mechanical equilibrium of the SMA wire.

The design of the system allows to introduce a congruence equation, that describes the kinematics of the problem, in the form of

$$\varepsilon = \frac{R(\frac{\pi}{2} - \theta)}{l_{in}} \tag{5}$$

where R is the pulley radius and l_{in} is the undeformed wire length. Equation 5 shows the link between the wire strain and the rotation angle, and it is needed to close the problem.

4. Results

The Brinson model is firstly implemented in the numerical analysis considering a temperature distribution on the wire that is uniform for each equilibrium state and, then, the model is expanded to consider a non-uniform temperature distribution.

4.1. Uniform temperature of the SMA wire

The temperature T is an input to the analysis. Considering the whole length of the wire, the temperature is increased (or decreased) by means of steps and is defined as

$$T^{(i)} = T_{in} + i\Delta T \tag{6}$$

where T_{in} is the initial temperature, i is the step number and ΔT is the temperature increment.

In addition to temperature, the Brinson model needs as input also the actual stress along the wire, which is related to the mechanical equilibrium. Then, to obtain the stress, the iterative process shown Figure 8 has been implemented. For a given temperature step i, the inputs for the analysis are the actual temperature $T^{(i)}$ and the stress $\sigma^{(i-1)}$ computed at the previous step. The Brinson model is applied and the strain $\varepsilon^{(i)}$ is calculated by the constitutive law. The kinematic equation allows the computation of $\theta^{(i)}$ and the mechanical equilibrium allows to compute the stress $\sigma^{(i)}$, that is used as input for the subsequent step.

The temperature of the wire is initially set to the surrounding environmental temperature $T_{in} = 20°\text{C}$. Then, the temperature is increased (heating process), step by step, until the martensite to austenite transformation is completed and the SMA σ–T state belongs to region 4. Then, the temperature is decreased (cooling process) up to the environmental temperature. The results of the numerical analysis are shown in figures 9 and 10 for what concern, respectively, the stress and rotation angle over the temperature. Two curves appear in each figure: the red curve is relative to the heating process, while the blue one describes the cooling process.

The SMA actuation allows the system to open and to close, along rotation angles greater than 80°; due to the different values of martensite start and finish temperature with respect to austenite start and finish temperatures, the opening and closing phases happens for different SMA wire temperatures.

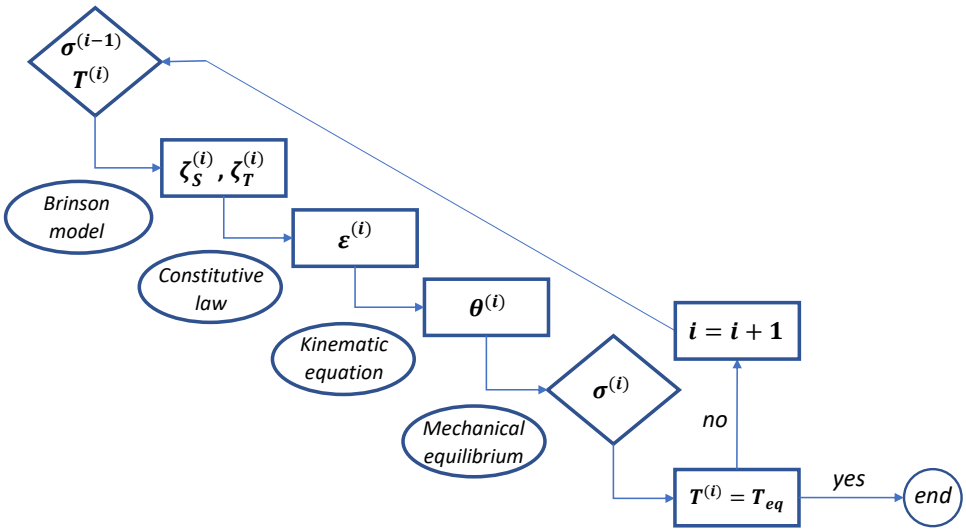

Figure 8. Uniform temperature model: flow diagram.

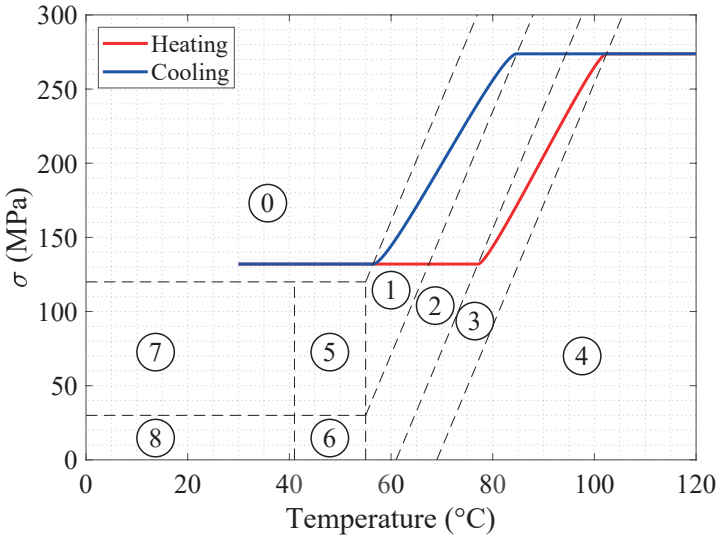

Figure 9. Uniform temperature model, heating and cooling processes: stress over temperature.

4.2. Non-uniform temperature of the SMA wire due to conductive heating

The previously described model is a useful prediction tool in the case of uniform heating or cooling of the SMA wire (e.g. obtained through Joule effect or by changing the environmental temperature). However, the proposed application differs from the widely studied cases in literature because the SMA wire receives localized thermal power from both the clamped ends. The temperature field along the wire is expected to be characterized by a spatial gradient. To simulate this behavior, the stationary temperature distribution is computed by the monodimensional fin thermal model with temperature imposed at both ends and convection along the wire. Figure 11 shows the computed temperature distribution setting 150°C to both ends and 5 W/(m^{2}K) as SMA convective heat transfer coefficient, while the conduction along the wire is assumed a function of the martensite fraction. In particular, the thermal conductivity is assumed to be constant before and after the transition region respectively (8 W/(mK) and

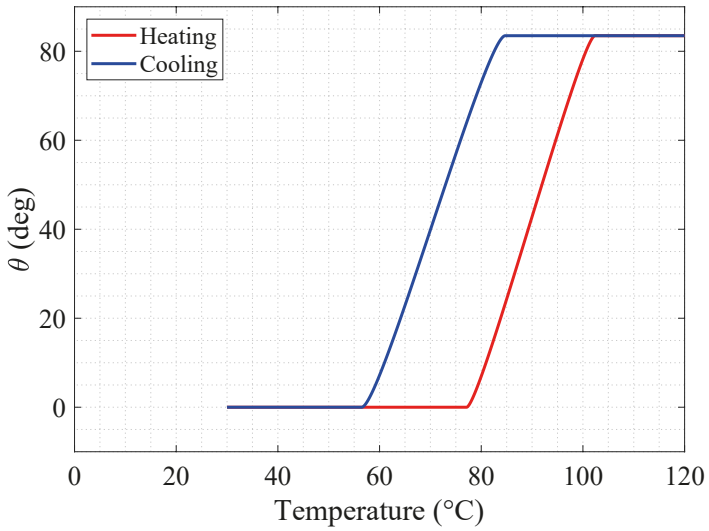

Figure 10. Uniform temperature model, heating and cooling processes: rotation angle over temperature.

18 W/(mK) for martensite and austenite, respectively), while varying linearly during the phase transformation.

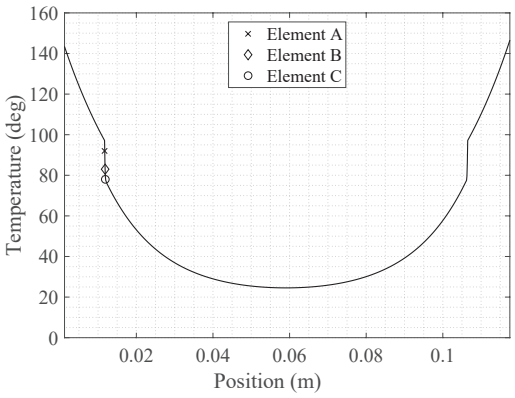

Figure 11. Temperature distribution along the wire for the temperature gradient model - Whole wire length.

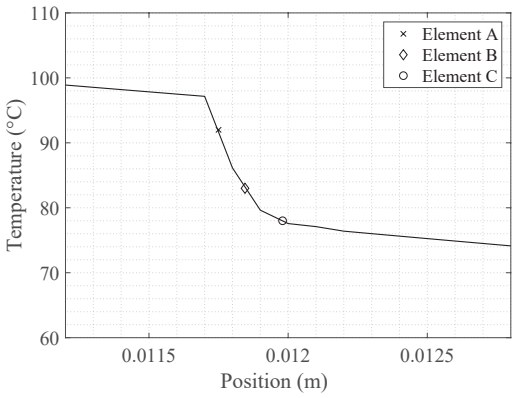

Figure 12. Temperature distribution along the wire for the temperature gradient model - Zoom on the phase transformation region.

The plot in figure 11 shows discontinuities in the derivative of the temperature distribution, caused by the variation of the conduction properties when the phase changes from martensite to austenite. Figure 12 shows a zoom on the plot of the temperature distribution in the transition zone.

In order to simulate the deformation, the wire is subdivided in smaller elements, in such a way that the temperature difference between one end of the element and the other one is less than or equal to 3°C. Following this lead, the wire is now subdivided in portions of variable length, and each portion presents a stationary temperature gradient from which the mean value is computed and associated to the relative element.

Once the stationary temperature of each element is known, a strategy similar to the one already described in the previous section is adopted. Considering each element j, in order to simulate the device closing operation, its temperature is varied step by step as follows

$$T_j^{(i)} = \min(T_{in} + i\Delta T, T_{j,fin}) \tag{7}$$

where T_{in} is the initial environmental temperature (constant for each element) and $T_{j,fin}$ is the final temperature of the $j-$th element, obtained from figure 11. Figure 13 shows the flow diagram that summarizes the model: for each step i and each element j, the actual element strain $\varepsilon_j^{(i)}$ is computed and used to obtain the overall wire strain $\varepsilon_{tot}^{(i)}$. The kinematic equation and the mechanical equilibrium are used to calculate the rotation angle $\theta^{(i)}$ and the actual stress $\sigma^{(i)}$ that will be the input for the following step.

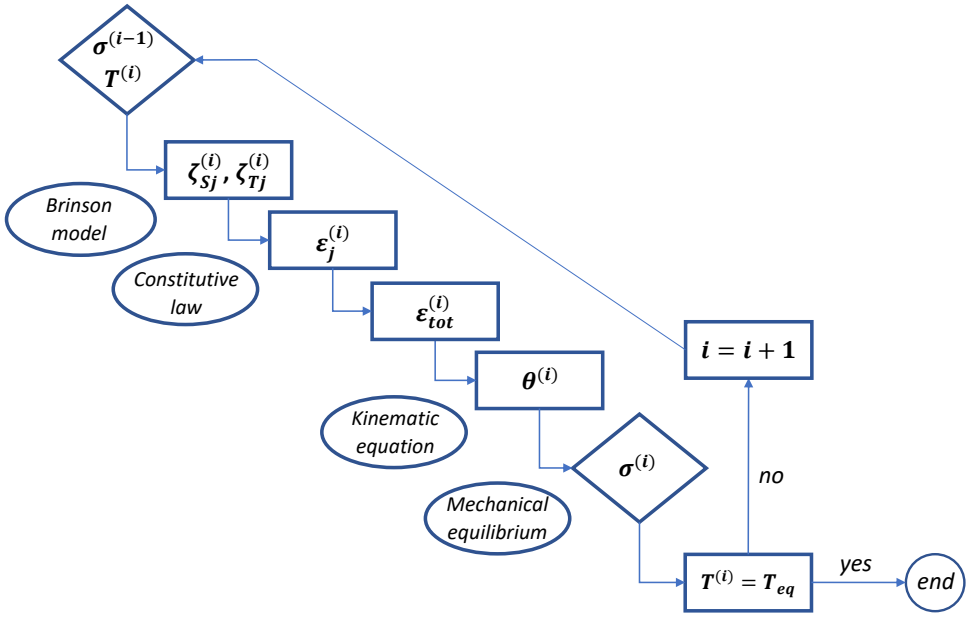

Figure 13. Temperature gradient model: flow diagram.

For the sake of conciseness the results refer only to the heating phase. In Figure 11 three elements are selected along the wire, Element A, Element B and Element C whose final temperature is 92 °C, 88 °C and 73 ° C respectively, to explain the different states at the end of the simulation. The same elements are identified also in figures 14–17, where the results of the simulation are plotted. In particular, figure 14 shows the region distribution (see figure 6) along the wire: Element A belongs to region 4 (pure austenite), Element C to region 2 (pure martensite during heating) while Element B belongs to the heating transformation region (region 3). Indeed, only the wire elements which belongs to region 4 have been able to perform the whole phase transformation from martensite to austenite, some elements performed only a partial transformation (as Element B) while many elements have not changed their phase transformation and are still in martensite phase (all the element which belong, at the end of the simulation, to region 2, region 1 and region 0). Figure 15 shows the stress-temperature history for the three elements: the final stress is obliviously the same for all the element but the final temperature is different and consequently the region which the elements belong to at the end of the simulation. Figure 17 and figure 16 show the martensite phase distribution and the element strain respectively along the wire: the central element (e.g. Element C) are still martensite at

the end of the simulation and do not contribute to the strain recovery, since their temperature is below the martensite to austenite transformation temperature for the stress which are subject to.

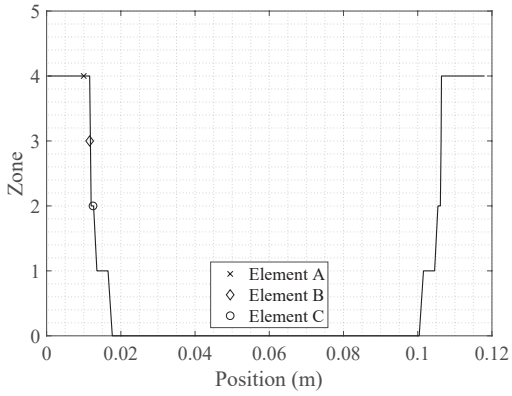

Figure 14. Region distribution along the SMA wire.

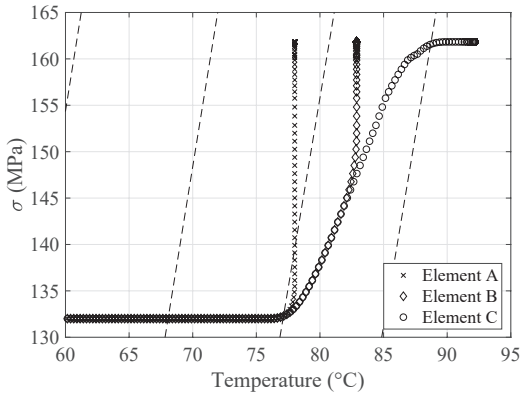

Figure 15. Stress vs Temperature plot.

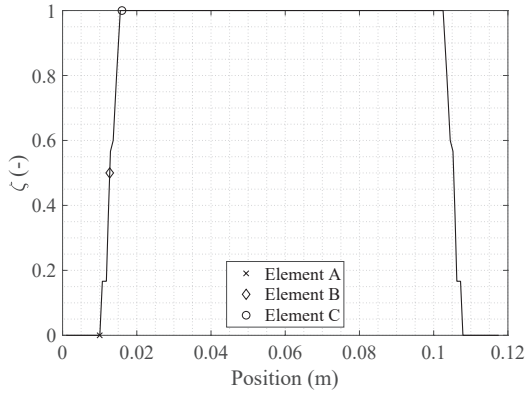

Figure 16. Martesite phase distribution along the SMA wire.

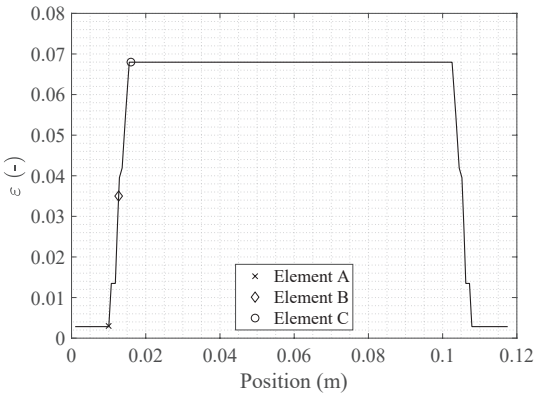

Figure 17. Strain distribution along the SMA wire.

For this reason, since only the end element (e.g. Element A) complete the austenite transformation and contribute to the wire strain recovery, only a part of the total strain of the wire is recovered and the rotation angle of the heat radiator is about 20 °.

5. Conclusions

In the present study a multifunctional structure for space engineering application, part of the TOPDESS project funded by ESA, has been proposed. The structure consists of a folded PHP heat exchanger which can be unfolded thanks to a SMA actuation system. Mechanical and thermal models were used to simulate the structural behavior of both the foldable PHP and the SMA wire, using the Brinson-Chung model. In particular two case-studies were considered: a reference case with a wire constant temperature, up to above the austenite finish temperature, and a further case having passive heating of the wire due to lumped heat sources at the wire ends and convection along the wire length, which produces a temperature gradient.

The feasibility study allowed to understand that metallic and foldable PHPs are feasible, using materials belonging to series 2000 and 7000 of Aluminium. With these choices, the adiabatic

section of the PHP can be shaped as a torsional spring, allowing rotations of about 90° without plastic strain.

The SMA actuation system based on NiTi wires is also feasible, allowing rotations of the system in the order of 90° if the wire is uniformly heated up to a temperature greater than the austenite finish temperature. The second case, referred to a passive heating of the SMA wire coupled with heat transfer devices, does not obtain a total opening of the system (rotation angle lower than 20°). A better thermal characterization of the specific NiTi alloy could refine these results.

Currently a prototype of the system is under construction to experimentally validate the concept of the system and the SMA model strategies.

References

[1] Lagoudas D C 2008 *Shape Memory Alloy: modeling and engineering applications* (Boston: Springer).

[2] Katayama T, Sugiyama Y, Kawashima S and Nishino K 1996 Shape memory alloy wire actuated hinge mechanism for deploying segmented panels *Bulletin of Osaka Prefecture University, Series A*, **45**, 119-124.

[3] Carpenter B F and Lyons J 2002 Lightweight Flexible Solar Array validation report *EO-1 First, NASA mission, validation report* .

[4] Vale Pereira P D, Chun K S, Contreras M M, Lindsay C, Kacker S, Huffman R, Haughwout C and Cahoy K 2002 *Folded Lightweight Actuator Positioning System (FLAPS)* 33^{rd} Annual AIAA/USU Conference on Small Satellites (Boston).

[5] Lan X, Leng J and Du S 2007 Design of a deployable antenna actuated by shape memory alloy hinge *Materials Science Forum*, **546–549** 1567-70.

[6] Maffiodo D and Raparelli T 2017 Design and realization of a flexible finger actuated by Shape Memory Alloy (SMA) wires *International Journal of Applied Engineering Research***12** 15635–43.

[7] Bertagne C L , Cognata T J, Sheth R B, Dinsmore C E, Hart D J 2017 Testing and analysis of a morphing radiator concept for thermal control of crewed space vehicles *Applied Thermal Engineering* **124** 986–1002.

[8] Guzik A and Benafan O 2018 Proceedings of the 44^{th} Aerospace Mechanisms Symposium (Cleveland) 2018–219914.

[9] Akizuki, Y, Nagano, H, Kinjo, T, Sawada, K, Ogawa, H, Takashima, T, Nishiyama, K, Toyota, H, Watanabe, K and Kuratomi, T, 2020 Development and testing of the re-deployable radiator for deep space explorer *Applied Thermal Engineering* **165** 114586

[10] M.H. Elahinia 2016 *Shape Memory Alloy Actuator: design, fabrication, and experimental evaluation* (Chicester: John Wiley & sons).

[11] Lexcellent C, Goo B, Sun Q P and Bernardini J 1996 Characterization, thermomechanical behaviour and micromechanical-based constitutive model of shape-memory Cu-Zn-Al single crystals *Acta Materialia* **44**, 3773–80.

[12] Levitas V and Stein E. 1997 Simple micromechanical model of thermoelastic martensitic transformations *Mechanics Research Communications* **24** 309–18.

[13] Levitas V and Ozsoy I 2009 Micromechanical modeling of stress-induced phase transformations. Part 1. Thermodynamics and kinetics of coupled interface propagation and reorientation *International Journal of Plasticity* **25** 239–80.

[14] Tanaka K 1986 A thermomechanical sketch of shape memory effect: onedimensional tensile behavior *Research Mechanicanical* **18** 251–63.

[15] Liang C and Rogers C A 1990 One-dimensional thermomechanical constitutive relations for shape memory material *Journal of Intelligent Material Systems and Structures* **1** 207–34.

[16] Brinson L C 1993 One-Dimensional Constitutive Behavior of Shape Memory Alloys: Thermomechanical Derivation with Non-Constant Material Functions and Redefined Martensite Internal Variable *Journal of Intelligent Material Systems and Structures* **4** 229–242.

[17] Boyd J G and Lagoudas D C 1996 A thermodynamical constitutive model for shape memory materials. part i. the monolithic shape memory alloy *International Journal of Plasticity* **12** 805–42.

[18] Chung J A, Heo J S and Lee J J 2006 Implementation strategy for the dual transformation region in the Brinson SMA constitutive model *Journal of Smart Materials and Structures* **16** N1.

[19] Bucchi F, Elahinia M, Forte P, Frendo F 2014 A Passive Magneto-Thermo-Mechanical Coupling Actuated by SMA Springs and MR Fluid *International Journal of Structural Stability and Dynamics* **14** 8.

[20] Krishnan V B 2004 *Design, Fabrication And Testing Of A Shape Memory Alloy Based Cryogenic Thermal Conduction Switch* (University of Central Florida:Master thesis).